J Mater Sci
DOI 10.1007/s10853-015-9158-y

CrossMark

50TH ANNIVERSARY

Fast-curing epoxy polymers with silica nanoparticles: properties and rheo-kinetic modelling

A. Keller[1,2] · K. Masania[2] · A. C. Taylor[1] · C. Dransfeld[2]

Received: 31 March 2015 / Accepted: 5 June 2015
© The Author(s) 2015. This article is published with open access at Springerlink.com

Abstract Fast-curing epoxy polymers allow thermoset parts to be manufactured in minutes, but the curing reaction is highly exothermic with heat flows up to 20 times higher than conventional epoxies. The low thermal conductivity of the polymer causes the mechanical and kinetic properties of parts to vary through their thickness. In the present work, silica nanoparticles were used to reduce the exotherm, and hence improve the consistency of the parts. The mechanical and kinetic properties were measured as a function of part thickness. The exothermic heat of reaction was significantly reduced with the addition of silica nanoparticles, which were well dispersed in the epoxy. The silica nanoparticles increased the Young's modulus linearly from 3.6 to 4.6 GPa with 20 wt% of silica, but the fracture energy was found to increase less than for many slow-curing epoxy resins, with values of 176–211 J m^{-2} being measured. Although there was no additional toughening, shear band yielding was observed. Further, the addition of silica nanoparticles increased the molecular weight between crosslinks, indicating the relevance of detailed cure kinetics when studying fast-curing epoxy resins. A model was developed to describe the increase in viscosity and degree of cure of the unmodified and the silica-modified epoxies. A heat transfer equation was used to predict the temperature and resulting properties through the thickness of a plate, as well as the effect of the addition of silica nanoparticles. The predictions were compared to the experimental data, and the agreement was found to be very good.

Introduction

Epoxy polymers have many applications, including in adhesives, coatings and fibre composite materials. Conventionally, such thermoset polymers are cured relatively slowly, but the demand for increased manufacturing throughput is driving cycle times down from hours or tens of minutes to several or a few minutes. Some of this reduction in cycle time can be partly achieved by reducing the time taken to fill the mould. For example, for liquid composite moulding processes, the time required for fibre impregnation can be greatly reduced by using through-thickness impregnation (e.g. by compression resin transfer moulding (CRTM) [1]). This approach reduces the impregnation length compared to standard in-plane infusion processes, and therefore reduces the impregnation time by orders of magnitude. However, curing is generally the rate-determining step in the manufacturing process, and so fast-curing epoxies are being developed.

Although the rheology and cure kinetics of slow-curing epoxies have been studied and modelled [2–5], the use of fast-curing systems gives new challenges [6, 7]. To achieve the short cure times the mould is pre-heated, so the degree of cure and viscosity of the epoxy evolve as a function of time whilst the mould is being filled, and so these must be considered as variables for flow modelling. The fast and highly exothermic nature of the curing also causes difficulties in measuring accurate experimental data. Yang et al. [6] found that the total heat of reaction from isothermal measurements decreases at higher temperatures because

✉ A. C. Taylor
a.c.taylor@imperial.ac.uk

[1] Department of Mechanical Engineering, Imperial College London, South Kensington Campus, London SW7 2AZ, UK

[2] Institute of Polymer Engineering, University of Applied Sciences and Arts Northwestern Switzerland FHNW, Klosterzelgstrasse 2, 5210 Windisch, Switzerland

Published online: 02 July 2015

the heat flow is not measured correctly in the initial stage of curing. To overcome this, Prime et al. [7] extrapolated isothermal curing curves from dynamic measurements for fast-curing resins.

This exothermic heat also has a significant impact on the manufacturing and properties of epoxy polymer or composite parts [8, 9]. The poor thermal conductivity of the epoxy results in a large temperature increase in the centre of the part (especially when thick), which gives a higher degree of cure in the centre than at the edges. Hence the glass transition temperature and the properties of the epoxy will vary through the thickness. The addition of ceramic particles will reduce the temperature exotherm and cure shrinkage, by reducing the volume of epoxy and increasing the thermal conductivity, as reported in [10]. For composite manufacturing, any such particles must be small such that they are not filtered out during infusion processes, for example silica nanoparticles [11].

The addition of particles can also improve the properties of the epoxy polymer. Although epoxies have high modulus, strength and temperature stability due to their highly cross-linked matrix structure, this structure makes the polymer relatively brittle. The fracture toughness of the epoxy can be increased by adding particles such as silica nanoparticles [12] or core–shell rubber nanoparticles [13]. Such silica nanoparticles give increases in stiffness, fracture energy [12, 14, 15] and cyclic-fatigue resistance [16]. It has been shown that these silica nanoparticles remain well dispersed in slow-curing epoxies [17].

This suggests that silica nanoparticles may be advantageous when manufacturing components using fast-curing epoxies, so the present work will investigate of the effects of silica nanoparticles on fast-curing resins by studying the curing behaviour, the rheological behaviour and the mechanical response. The rheology and kinetics will be modelled, and the variation in the glass transition temperature through the thickness of plates will be predicted and compared with experimental results.

Materials

The epoxy resin used was a diglycidyl ether of bisphenol A (DGEBA) epoxy with an epoxy equivalent weight (EEW) of 181.5 g eq^{-1}, "XB 3585" from Huntsman Advanced Materials, Switzerland. The curing agent was a mixture of diethylenetriamine and 4,4′-isopropylidenediphenol, "XB 3458" from Huntsman Advanced Materials, and was used at a stoichiometric ratio of 100:19 by weight of epoxy to hardener.

The silica (SiO_2) nanoparticles were supplied as a masterbatch, "Nanopox F400" from Evonik Hanse, Germany, with 40 wt% of silica nanoparticles predispersed in DGEBA (EEW = 295 g eq^{-1}) with a mean diameter of 20 nm [18]. Formulations with up to 20 wt% of silica nanoparticles (20 N) were used for the mechanical and fracture tests, with some additional measurements with up to 35.8 wt% of silica nanoparticles (35.8 N).

For comparison, a conventional slower-curing epoxy was also used. This was "HexFlow RTM6", from Hexcel, UK, which comprises a tetrafunctional epoxy resin, tetraglycidyl 4-4′ diaminodiphenylmethane, and two amine hardeners: 4,4′-methylene-bis(2,6-diethylanaline) and 4,4′-methylene-bis(2,6-diisopropylaniline).

Experimental methods

Thermal mechanical characterisation

Two differential scanning calorimeters were used for the thermal characterisation. Firstly, measurements were performed using a TA Q1000 with a cooler unit that enabled measurements below room temperature. The glass transition temperatures, T_g, of the uncured and cured polymers were measured using a sample mass of 2 mg and heating rate of 10 °C min^{-1}. Modulated measurements (±0.30 °C every 15 s) were conducted to determine the glass transition temperature and the residual heat of reaction for the partially cured resin. Secondly, isothermal and dynamic measurements to determine the total heat of reaction were conducted using a Mettler DSC 1 using 5 mg of resin in "tzero" aluminium pans as this DSC allows manual opening of the pre-heated furnace. All the measurements were conducted using a nitrogen sample purge flow to reduce oxidation of the resin.

The molecular weight between cross-links, M_c, was calculated using the relation proposed by Nielsen [19] as

$$M_c = \frac{3.9 \times 10^4}{T_g - T_{g0}}, \quad (1)$$

where T_{g0} is the glass transition temperature of the linear polymer, and was taken as 55 °C from Bellenger and Verdu [20]. The validity of this method has been shown previously in [21] and it was assumed that the silica nanoparticles do no interact with the polymer network, as was shown by the constant T_g of silica nanoparticle-modified slow-curing epoxies [12].

Rheological study

A PAAR Physica MCR 302 plate–plate rheometer or a TA AR 200 EX plate–plate rheometer was used to measure the change in viscosity of the unmodified and the silica nanoparticle-modified epoxies. Disposable aluminium plates of 25 mm diameter were used, and the gap between

the plates was set to 1 mm. A strain of 1 % and an angular frequency of 10 s^{-1} were used.

Manufacturing

Bulk epoxy plates of 3, 4 and 6 mm thickness were cast in 8-mm-thick aluminium moulds, which were pre-heated to 80 °C. The plates were cured in an oven at 80 °C for 12 min. This slightly slower cure-cycle was preferred to prevent the very strong exothermic reaction and decomposition, which may occur for 6 mm plates manufactured at 100 °C.

Microstructure

The morphology of the unmodified and silica nanoparticle-modified epoxies was observed using atomic force microscopy (AFM). Height and phase images were obtained using a MultiMode scanning probe microscope from Veeco, USA, with a NanoScope IV controller and an E scanner. The samples were prepared at room temperature using a PowerTome XL cryo-microtome form RMC Products, USA.

Modulus and yield behaviour

The Young's modulus, E_t, of the bulk unmodified and silica nanoparticle-modified epoxies were determined using uniaxial tensile tests according to BS ISO 572-2 [22]. Dumbbell specimens (type 1BA) were machined from the epoxy plates using a water-jet cutter. The tests were performed using an Instron 5584 universal testing machine, with a gauge length of 25 mm and a displacement rate of 1 mm min^{-1}. An Instron 2620-601 dynamic extensometer was used to measure the strain. A minimum of five samples were tested for each formulation.

Compression properties

Plane strain compression (PSC) tests were performed to determine the compressive properties of the polymers as proposed by Williams and Ford [23], and as discussed in [12]. Polished specimens with dimensions of $40 \times 40 \times 3$ mm^3 were compressed between two parallel dies of 12 mm width using an Instron 5585H at a displacement rate of 0.1 mm min^{-1}.

An unmodified epoxy sample was interrupted post-yield, i.e. in the strain softening region, then sectioned and polished. This sample was examined using optical microscopy between crossed polarisers to confirm that shear band yielding was present.

Fracture properties

Single-edge-notched bending (SENB) tests were performed according to ASTM D5045 [24] to determine the plane-strain fracture toughness, K_C, and the fracture energy, G_C, of the unmodified and of the silica nanoparticle-modified epoxies. Sample dimensions of $60 \times 12 \times 6$ mm^3 with a V-notch of 4 mm in depth were water-jet cut. A sharp pre-crack was obtained by tapping a new razor blade, cooled with liquid nitrogen, into the notch. An Instron 5584 was used to perform the tests at a constant displacement rate of 1 mm min^{-1}.

Cure kinetic modelling

Determination of glass transition temperature

Differential scanning calorimetry (DSC) with a heating rate of 10 °C min^{-1} was used to obtain the glass transition temperature, T_g. The value for the uncured epoxy, T_{g0}, was measured to be -27.0 ± 0.5 °C, and for the cured epoxy, $T_{g\infty}$, to be 121 ± 1 °C. These values remained constant with the addition of silica nanoparticles, indicating no kinetic effect, and hence there appears to be no chemical interaction between the particles and the epoxy, as previously reported [12].

Determination of total heat of reaction

The total heat of reaction, ΔH_{tot}, was determined using dynamic measurements with heating rates, dT dt^{-1}, from 10 to 30 °C min^{-1} at 5 °C min^{-1} intervals between room temperature until the material was fully cured. The mean value was determined from the three highest ΔH_{tot} readings. For the unmodified epoxy ΔH_{tot} was measured to be 494 ± 4 J g^{-1}.

Measurements were performed for 10, 20, 25 and 35.8 wt% of silica (where 35.8 wt% is the maximum possible amount of silica in the epoxy when mixed with the curing agent). The addition of silica nanoparticles reduces the mass of the epoxy matrix, leading to a linear reduction ($m = -4.84$ J g^{-1} wt%) of heat flow proportional to the wt% of silica nanoparticles.

Isoconversion

Isothermal cure curves were determined from the dynamic measurements using the model-free kinetics (MFK) method proposed by Vyazovkin [25, 26]. This method has previously shown excellent agreement with measured data and was found to be superior compared to other studied isoconversion methods [25, 27, 28].

Vyazovkin [26] defined the time to reach a degree of cure, t_α, for a given temperature, T_0, as follows:

$$t_\alpha = \frac{J[E_a, T(t_\alpha)]}{\exp\left(\frac{-E_a}{RT_0}\right)}, \quad (2)$$

where E_a is the activation energy, R is the universal gas constant and

$$J[E_a, T(t_\alpha)] \equiv \int_{t_{\alpha-\Delta\alpha}}^{t_\alpha} \exp\left[\frac{-E_a}{RT_i(t)}\right] dt, \quad (3)$$

where E_a minimises

$$\Phi(E_a) = \sum_{i=1}^{n} \sum_{j\neq 1}^{n} \frac{J[E_a, T_i(t_\alpha)]}{J[E_a, T_j(t_\alpha)]}. \quad (4)$$

Isothermal measurements

The fast-curing nature of the epoxy causes several difficulties when conducting isothermal measurements using DSC. One method is to equilibrate the sample and the furnace at room temperature, and then to heat as fast as possible to the desired temperature. This method was found to be unsuitable for this fast-curing epoxy, as the resin cured partially before the heat flow was correctly measured at the set temperature, even with heating rates of up to 500 °C min^{-1}.

An alternative method is to preheat the furnace of the DSC, and then to place the sample inside. Approximately, 3–4 s of data were lost while the DSC chamber closed and began recording the heat flow. This method could be used with the Mettler DSC 1. Despite opening the device, the DSC was able to maintain a constant furnace temperature.

The heat flow was measured for temperatures from 60 to 110 °C, at 10 °C intervals. Measurements for the unmodified epoxy are shown in Fig. 1. Data were recorded until a proper baseline was reached. The reaction rates peak at the same degree of cure ($\alpha = 0.1$) for all isothermal measurements up to 100 °C. For higher temperatures, the peak was observed at a higher degree of cure as the DSC was not able to resolve the initial part of the curing reaction correctly due to the reaction progressing too quickly.

The maximum heat flow shows a relatively high magnitude compared to standard-curing epoxies. At 60 °C a maximum heat flow of 0.508 W g^{-1} is reached, increasing to 6.21 W g^{-1} at 100 °C (the upper processing temperature). In comparison, the HexFlow RTM6, a commonly used epoxy in the aerospace industry, has a maximum heat flow of 0.353 W g^{-1} at a cure temperature of 180 °C, i.e. a factor of 20 lower than the epoxy in this study. The measurements were repeated for the epoxies containing 10 and 20 wt% of silica nanoparticles, which again showed a decreased heat flow and total heat of reaction. The heat flow for isothermal conditions at 100 °C is shown in Fig. 1 (inset), and the reduction in heat flow can be seen clearly.

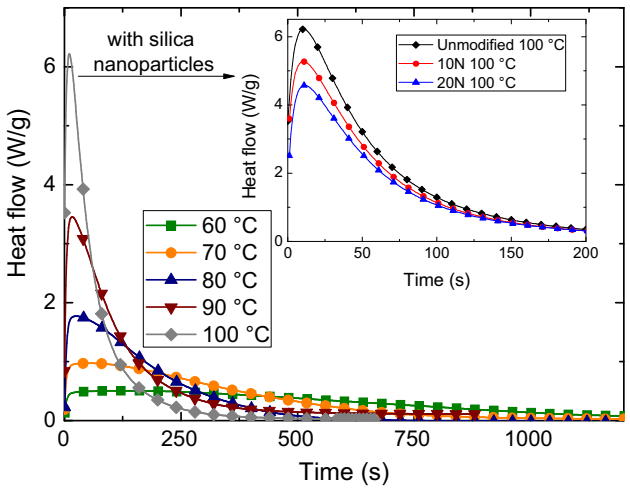


Fig. 1 Heat flow for isothermal measurements of the unmodified epoxy and (*inset*) measurements at 100 °C for the unmodified, 10 and 20 wt% silica-modified epoxies

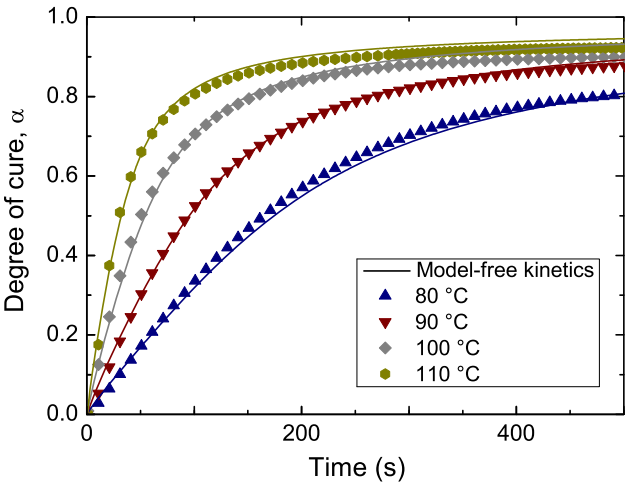


Fig. 2 Comparison between isothermal measurements (*points*) and modelled curves (*lines*) using the model-free kinetics approach from dynamic measurements for the unmodified epoxy

Comparison of isoconversion and measurement

The measured data and the isoconversion curves using the MFK approach from Eq. (2) were compared for temperatures from 80 to 110 °C, as shown in Fig. 2. The degree of cure progression shows good agreement between the measured and modelled data, especially in the initial stage of the curing reaction. However, the model overpredicts the degree of cure over the whole temperature range. The gap

between the measurement and the model towards the end of the conversion curves becomes larger with increasing temperature. This is due to the loss of data in the initial stage of the measurement before the DSC was able to record the heat flow correctly. This was further verified by noting that with increasing temperature more data were lost.

Kinetic modelling

The degree of cure, α, can be calculated for every time, t, during the cure reaction using

$$\mathrm{d}\alpha = \frac{\int_{t_1}^{t_2} \frac{\mathrm{d}H}{\mathrm{d}t}}{\Delta H_{\mathrm{tot}}}, \tag{5}$$

where $\mathrm{d}H\ \mathrm{d}t^{-1}$ is the measured heat flow in W g^{-1}, and ΔH_{tot} is the total heat of reaction in J g^{-1} from "Determination of total heat of reaction" section.

The heat flow and total heat of reaction decreased in proportion to the amount of silica, leading to identical conversion curves for all formulations that were studied. The reaction rate, $\mathrm{d}\alpha/\mathrm{d}t$, is proportional to the heat flow,

$$\frac{\mathrm{d}\alpha}{\mathrm{d}t} = \frac{\frac{\mathrm{d}H}{\mathrm{d}t}}{\Delta H_{\mathrm{tot}}}. \tag{6}$$

As described by Bailleul et al. [29], the reaction rate can be modelled as a function of the temperature and the degree of cure using

$$\frac{\mathrm{d}\alpha}{\mathrm{d}t} = k(T)G(\alpha), \tag{7}$$

where

$$k(T) = k_1 e^{\left(-E_1\left(\frac{T_{\mathrm{ref}}}{T}-1\right)\right)} \tag{8}$$

and

$$G(\alpha) = \sum_{i=0}^{m} G_i \alpha^i, \tag{9}$$

where k_1 is the frequency factor of the cure reaction, E_1 is the activation energy, T_{ref} is a randomly chosen temperature and G_i is a polynomial function.

Ruiz and Trochu [30] have extended the Bailleul model by a third term to consider the effects of glass transition temperature on the reaction rate by

$$K_3(T,\alpha) = (\alpha_{\max}(T) - \alpha)^n \tag{10}$$

with

$$n = f(T), \tag{11}$$

where $\alpha_{\max}$ is the maximum degree of cure for isothermal curing and n is the power exponent which depends on temperature, leading to the following model:

$$\frac{\mathrm{d}\alpha}{\mathrm{d}t} = k_1 e^{\left(-E_1\left(\frac{T_{\mathrm{ref}}}{T}-1\right)\right)} \sum_{i=0}^{m} G_i \alpha^i (\alpha_{\max}(T) - \alpha)^n. \tag{12}$$

The polynomial term is normalised to 1 at the maximum reaction rate. The reaction rate at this point can be modelled solely by Eq. (8).

The maximum degree of cure, $\alpha_{\max}$, was determined from the isothermal and ensuing modulated measurements. The values of $\alpha_{\max}$ determined from the dynamic modulated measurements were generally higher compared to the isothermal measurements. This difference was caused by the loss of data in the initial part of the measurement during the isothermal runs.

Therefore, to avoid this error due to onset of cure before data recording and subsequent baseline selection to measure heat flow, models for $\alpha_{\max}$ were developed using the modulated measurements,

$$\alpha_{\max} = \frac{T_{\mathrm{c}} - T_{\mathrm{g0}}}{(T_{\mathrm{c}} - T_{\mathrm{g0}})(1-\mu) + (T_{\mathrm{g}\infty} - T_{\mathrm{g0}})\mu}, \tag{13}$$

where T_{c} is the cure temperature, T_{g0} is the glass transition temperature of the uncured resin, $T_{\mathrm{g}\infty}$ is the glass transition temperature of the cured resin, and μ is a fitting parameter.

The parameters of the Arrhenius term were determined by normalising the polynomial term to 1 at the point of the maximum reaction rate, occurring at a degree of cure of 0.1.

$$\frac{\mathrm{d}\alpha}{\mathrm{d}t} = k_1 \mathrm{e}^{\left(-E_1\left(\frac{T_{\mathrm{ref}}}{T}-1\right)\right)} 1. \tag{14}$$

The reference temperature, T_{ref}, was set to 350 K, which lies in the middle of the measured range. The natural logarithm of Eq. (14) leads to a linear function. The activation energy, E_1, was obtained from the slope of the linear fit and the frequency factor, k_1, equals the exponential function of the intercept.

With the Arrhenius and the $\alpha_{\max}$ terms solved, the parameters for the polynomial term were determined using

$$\frac{\frac{\mathrm{d}\alpha}{\mathrm{d}t}}{k_1 \mathrm{e}^{\left(-E_1\left(\frac{T_{\mathrm{ref}}}{T}-1\right)\right)}} = \sum_{i=0}^{m} G_i \alpha^i (\alpha_{\max}(T) - \alpha)^n. \tag{15}$$

The polynomial term was found to be a 4th order polynomial divided by a second-order polynomial, using a least square fit, as

$$G(\alpha) = \frac{G_1\alpha^4 + G_2\alpha^3 + G_3\alpha^2 + G_4\alpha + G_5}{G_6\alpha^2 + G_7\alpha} \tag{16}$$

and reaction exponent n, using

$$n = n_s T_{\mathrm{c}} + n_i. \tag{17}$$

The model from Eq. 13, using the parameters shown in Table 1, gives good agreement with the dynamic measurements, as shown in Fig. 3a, with R^2-values between

Table 1 Fitting parameters for the cure kinetic model

Name	Symbol	Value
Polynomial parameter	G_1	−1351
Polynomial parameter	G_2	−2678
Polynomial parameter	G_3	10194
Polynomial parameter	G_4	4338
Polynomial parameter	G_5	−5.208
Polynomial parameter	G_6	587
Polynomial parameter	G_7	4570
Reaction exponent factor slope	n_s	0.018
Reaction exponent factor intercept	n_i	−5.2367
Frequency factor	k_1 (s^{-1})	0.00309
Activation energy	E_1	22.28
Reference temperature	T_{ref} (K)	350
T_g of the uncured resin	T_{g0} (K)	246.15
T_g of the cured resin	$T_{g\infty}$ (K)	394.4
Parameter for α_{max} model	μ	0.32

0.995 and 0.999. The model for the isothermal measurements showed a less good agreement than that for the dynamic measurements. For higher temperatures (80–100 °C), the initial curing is modelled well. However, the model overshoots the measured data as the curing reaction starts before the heat flow is measured by the DSC. This effect increases at higher temperatures, which is reflected in the model, illustrated in Fig. 3b with R^2-values between 0.981 and 0.997.

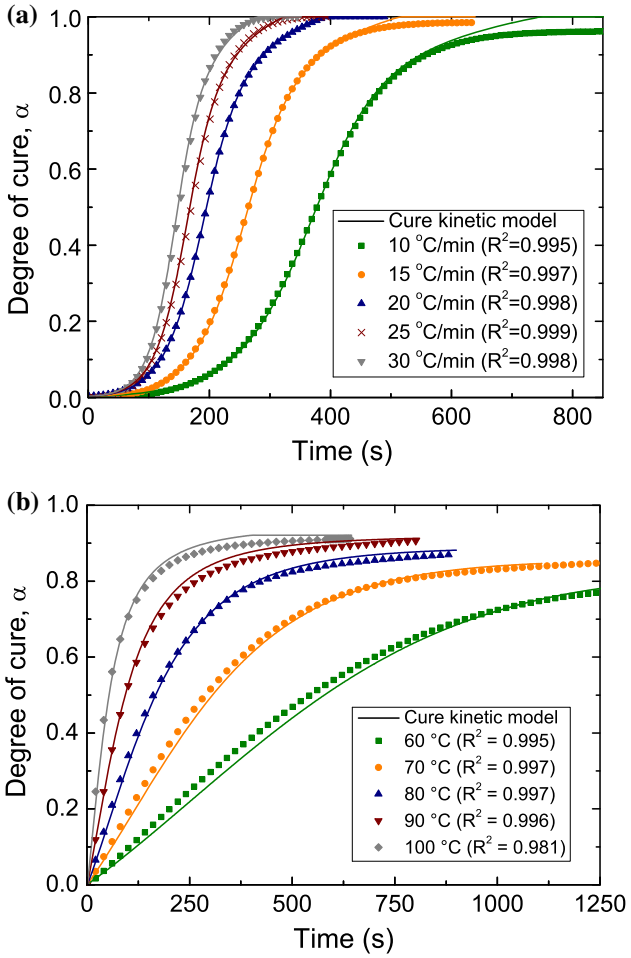


Fig. 3 Cure kinetic model for **a** dynamic measurements and **b** isothermal measurements of the unmodified epoxy

Glass transition modelling

The glass transition temperature, T_g, was modelled as a function of the degree of cure, α, using the DiBenedetto model [31]

$$T_g = T_{g0} + \frac{(T_{g\infty} - T_{g0})\lambda\alpha}{1 - (1-\lambda)\alpha}, \tag{18}$$

where T_{g0} and $T_{g\infty}$ are the glass transition temperature of the uncured and the fully cured material, respectively, from "Determination of glass transition temperature" section, and λ is a fitting parameter. The results are shown in Fig. 4a.

Measurements were obtained using a modulated DSC set-up. The T_g was measured directly from the reversible heat flow, and α was determined from the residual heat of reaction from the irreversible heat flow.

Heat transfer modelling

During the curing of an epoxy polymer, exothermic heat is created during the crosslinking reaction. With fast-curing epoxies, this exothermic heat leads to a large overshoot in the resin temperature compared to the mould temperature. Hence, the curing reaction cannot be assumed to occur at the mould temperature. The heat conduction model was solved in one dimension to account for a thickness-dependant temperature overshoot to give

$$\rho_r H_{tot}\frac{d\alpha}{dt} + k_{xx}\frac{\partial^2 T}{\partial x^2} = \rho C_p \frac{\partial T}{\partial t}, \tag{19}$$

where ρ_r is the resin density, ρ is the density of the composite resin, H_{tot} is the total heat of reaction from "Determination of total heat of reaction" section, $d\alpha\ dt^{-1}$ is the modelled reaction rate from Eq. (12), k_{xx} is the thermal conductivity and C_p is the specific heat capacity of the epoxy resin.

Finite element approach

Equation (19) was discretised using the finite element method with linear elements according to [8, 32], leading to an equation in the form

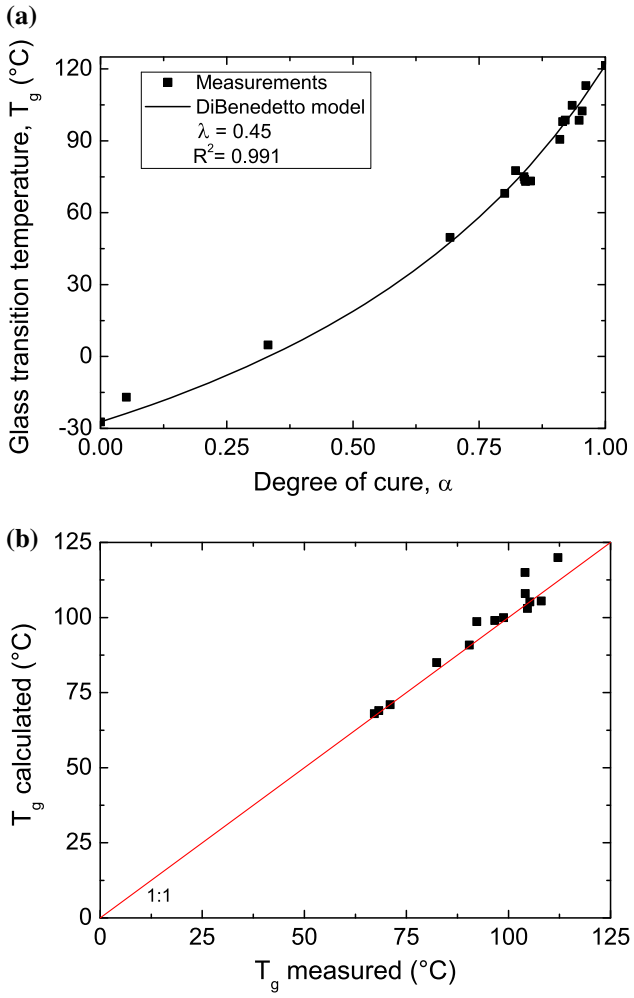


Fig. 4 **a** Glass transition temperature, T_g, as a function of degree of cure, α, compared to the DiBenedetto model [31] (*line*), and **b** comparison of measured and modelled T_g

$$[C]\{\dot{T}\} + [K]\{T\} - \{F\} = 0, \tag{20}$$

where $[C]$ is the thermal capacity matrix, $\{T\}$ is the temperature vector, $[K]$ is the thermal conductivity matrix and $\{F\}$ is the thermal load vector due to chemical reaction of the resin, with

$$[C] = \int_1 \rho C_p [N]^T [N] \mathrm{d}x \tag{21}$$

$$[K] = \int_1 k_{xx} [\dot{N}]^T [\dot{N}] \mathrm{d}x \tag{22}$$

$$\{F\} = \int_1 [N]^T \rho_r H_{tot} \frac{\mathrm{d}\alpha}{\mathrm{d}t} \mathrm{d}x, \tag{23}$$

where $[N]$ is the shape function.

A finite difference scheme was used for time discretisation [32],

$$([C] + \theta \Delta t[K])\{T\}^{n+1} = ([C] - (1-\theta)\Delta t[K])\{T\}^n + \Delta t\Big(\theta\{F\}^{n+1} + (1-\theta)\{F\}^n\Big), \tag{24}$$

where θ is a parameter to define the art of the scheme, chosen as 0.5 for a semi-implicit scheme, and Δt is the time step. For small time steps, the thermal load vector can be approximated by

$$\{F\}^{n+1} \approx \{F\}^n \tag{25}$$

which leads to

$$([C] + \theta \Delta t[K])\{T\}^{n+1} = ([C] - (1-\theta)\Delta t[K])\{T\}^n + \Delta t\{F\}^n. \tag{26}$$

Initial conditions

The polymer plates were cast in 8-mm-thick aluminium moulds. The values for the density, thermal conductivity, k, and specific heat capacity, C_p, of the materials which were used to solve Eq. (26), are summarised in Table 2, where the total heat of reaction was discussed in "Determination of total heat of reaction" section. After a convergence analysis, ten nodes per mm were used in the finite element analysis, where the time step was varied depending on the cure time, to produce approximately 3000 data points. The initial temperatures of the mould and epoxy were set to identical values, assuming that the resin heats up quickly during casting. Then, through internal heat generation during curing, the thermal heat vector $\{F\}$ was calculated to produce exothermic energy, resulting in an increase in the resin temperature and subsequently the mould temperature via conduction. The heat transfer between the mould and oven via convection was considered to be small and therefore neglected.

The predicted temperature distribution across the aluminium mould and the resin (a 6-mm-thick unmodified epoxy plate in this case) is shown in Fig. 5. At time $t = 0$ s, a stable temperature distribution was given as per boundary conditions. Over time, the internal heat was generated and conducted into the aluminium mould, which was predicted to increase in temperature by about 7 °C during the approximately 60 s that were described. Large temperature variations across the thickness of the epoxy plate were predicted, with a significantly higher temperature in the centre of the epoxy plate. Thereafter, the temperature decreased back to oven temperature, and the heat was dissipated slowly because convection between the oven and mould was not described in the model.

The specific heat capacity did not change significantly with the addition of 20 wt% silica nanoparticles (1700 vs.

Table 2 Values used for heat transfer modelling

	Aluminium	Unmodified (density of epoxy in formulation)	10 N (density of epoxy in 10 N formulation)	20 N (density of epoxy in 20 N formulation)
Density (kg m^{-3})	2700	1194	1247	1301
Density of epoxy (kg m^{-3})	–	1194	1185	1176
Thermal conductivity, k (W m^{-1} °C)	135	0.20 [33]	0.23 [33]	0.26 [33]
Specific heat capacity, C_p (J kg^{-1} °C)	1000 [37]	1700	1700	1700

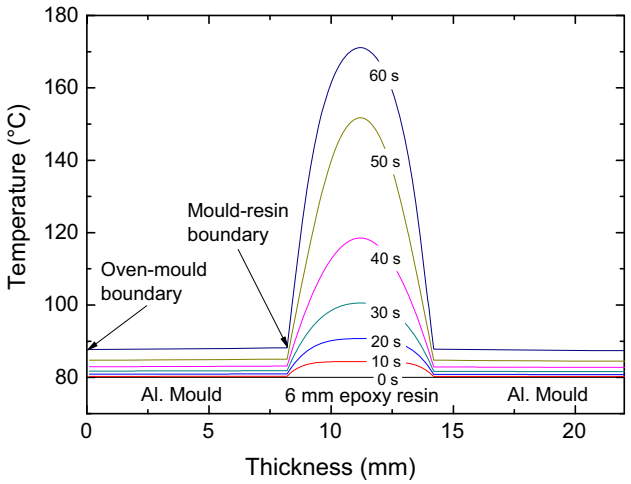


Fig. 5 Modelled temperature distribution across the thickness of the aluminium mould and 6-mm epoxy resin plate, cured at an oven temperature of 80 °C

1600 J kg^{-1} °C) and hence was kept constant. The values of k increased from 0.2 for the unmodified epoxy to 0.23 with 10 wt% and 0.26 for 20 wt% silica nanoparticles according to [33].

Comparison to experimental data

Equation (26) was solved using discretisation to predict the progression of the temperature, degree of cure and glass transition temperature during cure. The resin temperature can overshoot the mould temperature significantly if a high mould temperature is used and/or thick plates are manufactured. For example, the temperature of a 3-mm plate manufactured with a mould temperature of 100 °C peaked at a temperature of 176 °C. This temperature peak occurs at the very beginning of the curing reaction, and results from the kinetics as the maximum reaction rate occurred at the initiation of cure, i.e. after 20 s for a 3-mm plate cured at 100 °C. Further, when the plate thickness was increased, the heat generated in the centre of the plate could not be dissipated easily due to the low thermal conductivity of the epoxy.

A comparison between the measured and modelled temperature progression is shown in Fig. 6 for four cases. There is a good agreement between the modelled and experimental temperature evolution for the 3-mm plates produced using a 50 °C mould, see Fig. 6a. The temperature difference of approximately 2 °C has no significant influence on the kinetics, as can be seen in Table 3 where there is good agreement between the measured and calculated T_g values.

A comparison of the exothermic temperature of a 4-mm-thick plate cured at 80 °C, measured 0.8 mm from the edge, and a 3-mm plate cured at 100 °C, measured in the centre, is shown in Fig. 6b. In both cases, a large temperature overshoot was measured and predicted. The temperature progression is replicated well at the edge of plates, as can be seen for the 4-mm plate at 80 °C. Measurements taken in the centre of the plates, such as for the 3-mm plate at 100 °C, show a slight delay after the temperature peaks, which leads to an overestimation of T_g. This is probably a result of the assumed constant thermal conductivity, which will increase slightly with increasing temperature.

As can be seen in Fig. 6a, the peak temperature is reduced with the addition of silica nanoparticles due to the reduced total heat of reaction. For a 3-mm plate manufactured with a mould temperature of 100 °C, the calculated peak temperature is reduced from 173 to 163 °C with 10 wt% and to 154 °C with 20 wt% of silica nanoparticles. This gives a more controllable manufacturing process with a reduced risk of epoxy decomposition and a lower T_g.

The T_g was calculated using the DiBenedetto model (Eq. 18), and was predicted to vary over the thickness of the plates. For example, a 6-mm plate manufactured at 80 °C has a T_g difference of 7 °C between the edge and the centre, see Table 3. For the experimental data, at least two measurements were conducted for each position, and the repeatability was found to be very good (within ±1 °C).

The higher values of T_g in the centre of the plate can be explained by the higher peak temperature. At the edges, the heat is transported away through the mould faster than in the centre of the plate. With increasing plate thickness, there is an increase in the temperature gradient over the thickness (an example is shown in Fig. 5) as well as an increase in the maximum temperature.

A comparison of the experimentally determined and modelled values for T_g is shown in Fig. 4b, and the values

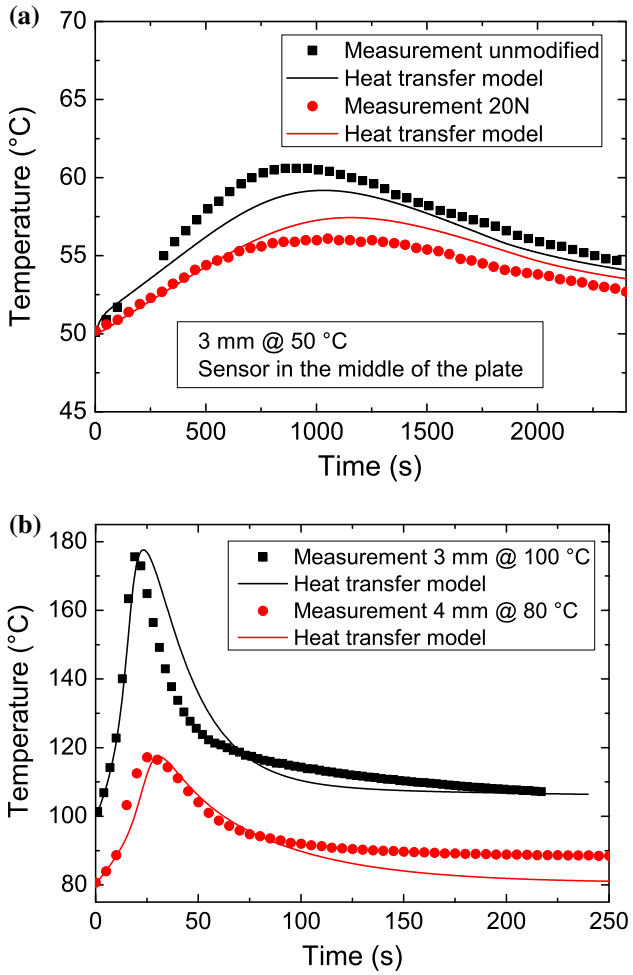


Fig. 6 Comparison of experimental (*points*) and modelled temperature progression (*line*) comparing **a** the effect of addition of silica nanoparticles and **b** variation of plate thickness and cure temperature, on the overall temperature exotherm

are summarised in Table 3. Measurements were taken from plates that were manufactured using different curing cycles, nanoparticle content, and positions through the thickness. The results generally agree well with the modelled data. As discussed above, the largest differences were for the centre of the 6-mm plates.

Rheological modelling

Shear rate dependency

The shear rate dependency was measured at room temperature, and a little shear thinning was observed when measurements were made between 100 and 1000 s^{-1}. The viscosity reduced from 3.75 Pas at a shear rate of 100 s^{-1} to 3.25 Pas at 1000 s^{-1}. The time between these two measurements was 100 s, during which the resin viscosity increased by 0.5 Pas resulting from the curing reaction, at a constant shear rate of 1 s^{-1}.

At the higher temperatures required for fast curing, the shear rate dependency became negligible as the curing reaction progressed very quickly, leading to a rapid increase in viscosity. For example, the viscosity increased from 0.5 to 10 Pas at 100 °C in 20 s for the unmodified formulation.

Isothermal measurements

Viscosity measurements for the unmodified and modified epoxies were obtained from 50 to 100 °C, at 10 °C intervals, using a plate–plate rheometer. Example results for 60 and 90 °C are shown in Fig. 7. The first measurement point

Table 3 Comparison of measured and modelled glass transition temperature, T_g

Material	Thickness (mm)	Position	Mould temperature (°C)	T_g measured (°C)	T_g calculated (°C)
Unmodified	3	Edge	50	71	71
10 N	3	Edge	50	68	69
20 N	3	Edge	50	67	68
Unmodified	4	Edge	60	82	78
Unmodified	4	Edge	80	90	91
Unmodified	4	Centre	80	92	99
Unmodified	6	Edge	80	105	103
10 N	6	Edge	80	99	100
20 N	6	Edge	80	97	99
Unmodified	6	Centre	80	112	120
10 N	6	Centre	80	104	115
20 N	6	Centre	80	104	108

occurs at between 30 and 60 s, which is the time taken from the moment when the resin first touches the preheated plate until the rheometer starts collecting data. A measurement at 60 °C was also performed using 35.8 wt% of silica nanoparticles for comparison, which resulted in a substantial increase in the initial viscosity, from 0.26 Pas for the unmodified resin to 1.49 Pas for the 35.8 wt% silica nanoparticle-modified epoxy. This viscosity increase was believed to occur due to a reduction of polymer chain mobility (non-linear effect) and would be expected to result in an increased fibre impregnation time during composite processing.

The times taken for the viscosity to reach 1 and 10 Pas at a given temperature, thus describing a hypothetical process window for fibre composite processing, for the unmodified epoxy, 10 and 20 wt% silica nanoparticle-modified epoxies, are compared in Fig. 8. At 60 °C, it takes about 170 s for the unmodified epoxy to reach 1 Pas, and at 90 °C this viscosity is reached in 84 s. At any temperature, the time taken to reach 1 Pas is roughly 7 s less for the 10 wt% and 10–15 s less for the 20 wt% silica nanoparticle epoxy compared to the unmodified epoxy, due to the increased viscosity. The time taken to reach 10 Pas was nevertheless similar for all three formulations, as the cure reaction kinetics dominated the evolution of the viscosity.

The time to reach a certain viscosity value can be modelled by fitting the following equation:

$$t = \mathrm{e}^{\frac{T-C}{B}}, \tag{27}$$

where T is the temperature, t is the time, B and C are fitting constants as summarised in Table 4.

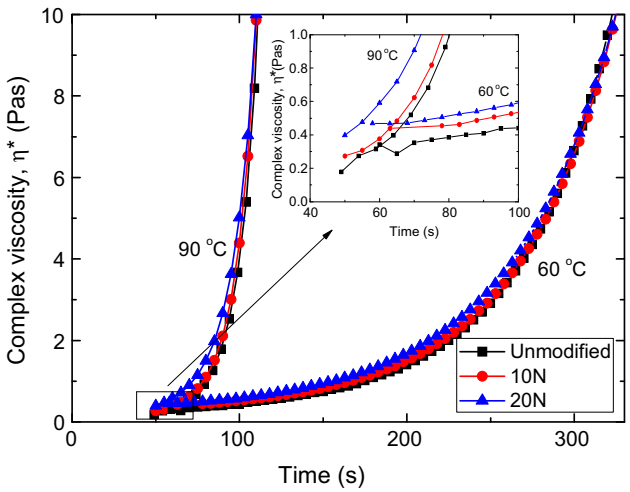


Fig. 7 Isothermal measurements at 60 and 90 °C. The initial viscosity increases with addition of silica nanoparticles (*inset*)

Rheological modelling

The model used or the rheological modelling is based on the Kiuna et al. approach [4] where the differential equation which describes the curing of the resin is

$$\frac{\mathrm{d}\alpha}{\mathrm{d}t} = \frac{k(T)}{g'(\alpha_2)}. \tag{28}$$

The model is based on the assumption that the viscosity can be modelled with the change in cure and where α_2 represents the dimensionless viscosity.

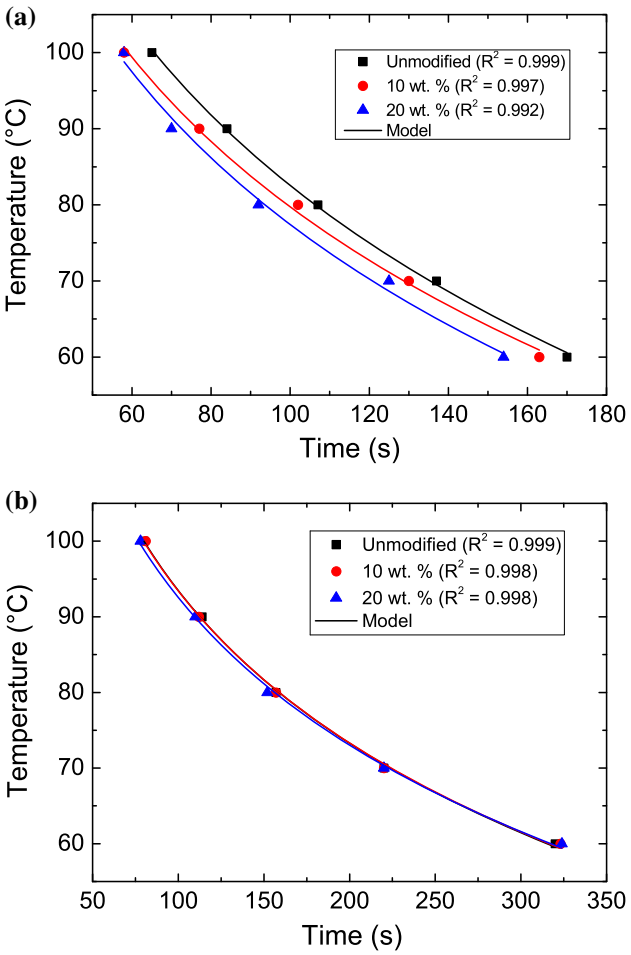


Fig. 8 Comparison of time to reach a viscosity of 1 Pas (**a**) and 10 Pas (**b**) for the unmodified and modified epoxies

Table 4 Parameters for the time to reach viscosities of 1 Pas and 10 Pas

	$B_{1\ \mathrm{Pas}}$	$C_{1\ \mathrm{Pas}}$	$B_{10\ \mathrm{Pas}}$	$C_{10\ \mathrm{Pas}}$
Unmodified	−41.4	273	−29.1	228
10 N	−38.5	257	−29.0	227
20 N	−39.2	258	−28.2	222

$$\alpha_2 = f(\tau) = \ln\left(\frac{\eta(T)}{\eta_0(T)}\right), \tag{29}$$

where η_0 is the viscosity of the uncured material and τ is the elapsed dimensionless cure time,

$$\tau = k(T)t \tag{30}$$

and

$$k(T) = \frac{1}{t_1}, \tag{31}$$

where t_1 is the time when α_2 becomes 1. Combining the derivative of the dimensionless viscosity, Eq. (28), with Eq. (29), leads to the following differential equation

$$\frac{\mathrm{d}\eta}{\mathrm{d}t} + \left(-\frac{k(T)}{g'(\alpha_2)} - \frac{\mathrm{d}\eta_o}{\mathrm{d}t}\frac{1}{\eta_o(T)}\right)\eta = 0. \tag{32}$$

For isothermal cure, the equation can be solved for the viscosity, which leads to

$$\eta(t,T) = \exp\left(\frac{k(T)}{g'(\alpha_2)}t\right)\eta_0. \tag{33}$$

The initial viscosity, η_0, and the advance of curing show an exponential dependency for different isothermal temperatures,

$$\eta_0(T) = A_1 \exp\left(\frac{E_1}{RT}\right) \tag{34}$$

and

$$k(T) = A_2 \exp\left(\frac{E_2}{RT}\right), \tag{35}$$

where R is the universal gas constant and where A_1, E_1, A_2 and E_2 are fitting parameters.

The next step is to determine the best fit for $g'(\alpha_2)$, for which an exponential approach was used

$$\alpha_2 = y_0 + A_3 \exp\left(\frac{\tau}{E_3}\right), \tag{36}$$

where y_0, A_3 and E_3 again are fitting parameters.

By substituting Eqs. (34–36) into Eq. (33), with the addition of a term to adjust for the shift in gel time, $(A_4\Delta T + E_4)$, the model for isothermal conditions becomes

$$\eta(t,T) = \exp\left(\frac{A_2 \exp\left(\frac{E_2}{RT}\right)}{E_3\frac{1}{A_3 \exp\left(A_2 \exp\left(\frac{E_2}{RT}\right)\frac{t}{E_3}\right)}}t(A_4T + E_4)\right) A_1 \exp\left(\frac{E_1}{RT}\right). \tag{37}$$

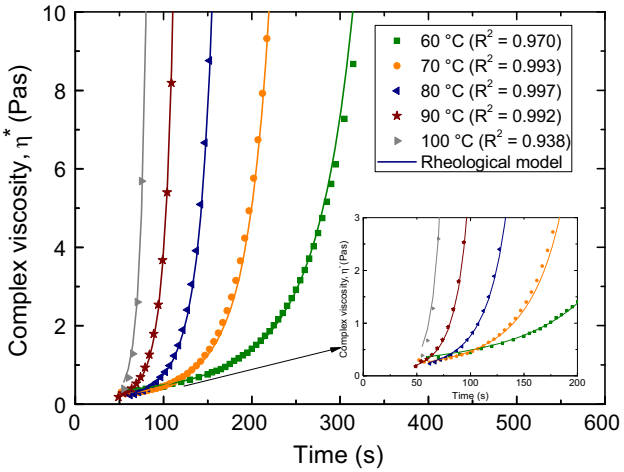


Fig. 9 Rheological model (*lines*) compared to experimental measurements (*points*) for the unmodified epoxy and (*inset*) low viscosity range

A comparison between measurements and the model for different isothermal temperatures of the unmodified epoxy is shown in Fig. 9. The model agrees well with the measured viscosity progression during the initial stage of the curing process. The modelling was repeated for the 10, 20 and 35.8 wt% silica nanoparticle-modified epoxies by modifying the values for A_1 and E_1, which represent the initial viscosity, as well as A_4 and E_4 to take into account the time shift. Intermediate silica contents can be interpolated from the values for these four formulations using the third-order polynomials shown in Table 5.

The calculated mean R^2 values of 0.978, 0.9774 and 0.965 describe the quality of fit for the unmodified, 10 and 20 wt% silica nanoparticle-modified epoxies, respectively, and thus the models represent the experimental data well.

To take the non-isothermal conditions during cure into account, either Eq. (32) can be used, or numerical integration of the time-dependent mathematical terms can be used to give

$$\eta(t,T) = \exp\left(\frac{\sum_i^n A_2 \exp\left(\frac{E_2}{RT}\right)t_i(A_4T + E_4)}{E_3\frac{1}{A_3 \exp\left(\sum_i^n A_2 \exp\left(\frac{E_2}{RT}\right)\frac{t_i}{E_3}\right)}}\right) A_1 \exp\left(\frac{E_1}{RT}\right). \tag{38}$$

A comparison of three heating rates for the unmodified epoxy is shown in Fig. 10, where the overall agreement was found to be good, with a slight delay of the viscosity increase (latency).

Table 5 Parameters used for the rheological model

Parameter	Unmodified epoxy	10 N	20 N	35.8 N
A_1	1.32×10^{-9}	6.81×10^{-10}	3.62×10^{-10}	1.37×10^{-10}
E_1	52,931	56,049	58,094	64,000
A_2	7518	7518	7518	7518
E_2	−38,710	−38,710	−38,710	−38,710
A_3	2.7	2.7	2.7	2.7
E_3	2.2	2.2	2.2	2.2
A_4	0.003	0.0046	0.006	0.007
E_4	−0.409	−1.047	−1.519	−1.732

The nanoparticle content-dependant equations to modify parameters are shown below (N is the wt% of silica)

$$A_1 = -2.5684 \times 10^{-14}N^3 + 2.3459 \times 10^{-12}N^2 - 8.4316 \times 10^{-11}N + 1.3156 \times 10^{-9}$$

$$E_1 = 0.36941N^3 - 16.444N^2 - 439.28N + 52931$$

$$A_4 = -5.5238 \times 10^{-8}N^3 + 6.5714 \times 10^{-7}N^2 - 1.5895 \times 10^{-4}N + 3.00 \times 10^{-3}$$

$$E_4 = 1.40495 \times 10^{-5}N^3 + 4.06514 \times 10^{-4}N^2 - 6.92301 \times 10^{-2}N - 0.409$$

Thermal and mechanical properties of the epoxy polymers

Thermal properties

The molecular weight between cross-links, M_c, can be calculated, as shown in Table 6 for the 6-mm plates that were manufactured at 80 °C. The observed variation through the thickness of the epoxy is apparent, where values of 780 and 684 g mol^{-1} were measured for the edge and centre of the unmodified epoxy, respectively. The value of M_c increased from 684 to 796 g mol^{-1} with the addition of 20 wt% silica nanoparticles.

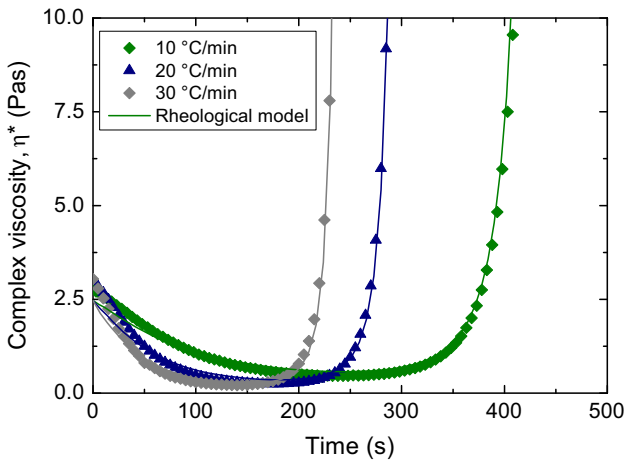


Fig. 10 Comparison of the developed rheological model (*lines*) to dynamic measurements (*points*) at different heating rates for the unmodified epoxy

Morphology

AFM was conducted on the unmodified epoxy and on the epoxies with 10 or 20 wt% silica nanoparticles. The resultant phase images are shown in Fig. 11. The planed surface of the unmodified sample was flat and featureless, see Fig. 11a, as expected for a homogenous thermoset polymer. The microtoming direction is shown on each image, and the scratches parallel to this direction are artefacts of the planning process. The images in Fig. 11b, c, show that there is a good dispersion and no significant size variation in the 20 nm diameter silica nanoparticles. The area disorder, $\overline{AD}$, was calculated for images of side length $L = 2.5$ μm and $L = 5$μm for the 10 wt% silica nanoparticle-modified epoxies using the methodology described in [34]. A value of $\overline{AD} = 0.4342$ and indicates that the particles in the test material are better dispersed than random, confirming that the silica is well dispersed.

Mechanical properties

The tensile Young's modulus, E_t, values of the unmodified and modified epoxies are summarised in Table 7. The modulus for the unmodified epoxy was measured to be 3.58 GPa. The addition of the nanoparticles increased the modulus as expected approximately linearly to 4.13 GPa with the addition of 10 wt% of silica, and to 4.62 GPa with the addition of 20 wt% of silica nanoparticles.

The true stress versus true strain curves were obtained using plane-strain compression tests for the unmodified and silica-modified epoxies, see Fig. 12. All the samples demonstrate strain softening after yield. The strain soft-

Table 6 Measured glass transition temperature and calculated molecular weight between crosslinks, M_c, of the epoxy polymers cured at 80 °C

	Thickness (mm)	Position	T_g measured (°C)	Molecular weight, M_c (g mol^{-1})
Unmodified	6	Edge	105	780
10 N	6	Edge	99	886
20 N	6	Edge	97	929
Unmodified	6	Centre	112	684
10 N	6	Centre	104	796
20 N	6	Centre	104	796

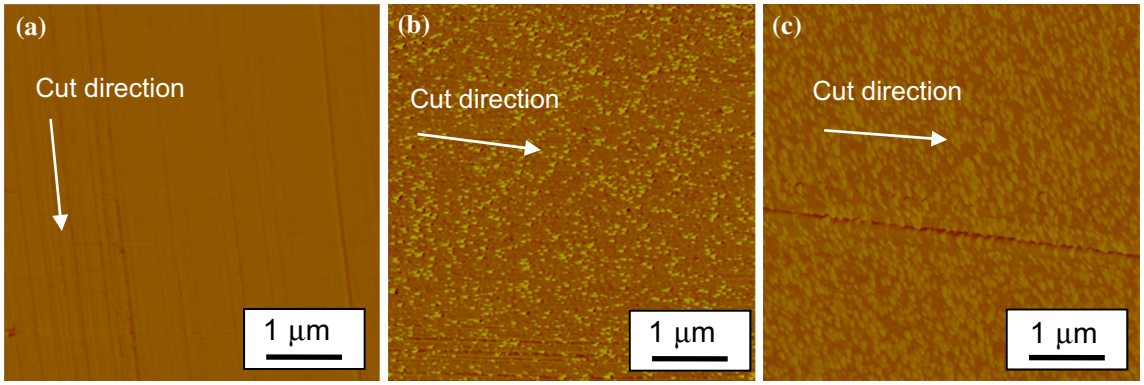


Fig. 11 Atomic force microscope phase images of the unmodified epoxy (**a**), 10 N (**b**) and 20 N (**c**) formulations. The *light yellow dots* are the silica nanoparticles (Color figure online)

Table 7 Mechanical properties of the epoxy polymers

	Tensile modulus, E_t (GPa)	Compressive modulus, E_c (GPa)	Compressive yield stress, σ_{yc} (MPa)	Compressive yield strain, ε_{yc} (−)	Fracture energy, G_C (J m^{-2})	Fracture toughness, K_C (MPa$\sqrt{m}$)
Unmodified	3.58 ± 0.11	2.14 ± 0.7	102 ± 11	0.10 ± 0.00	177 ± 35	0.85 ± 0.09
10 N	4.13 ± 010	2.18 ± 0.1	102 ± 1	0.08 ± 0.00	176 ± 15	0.91 ± 0.04
20 N	4.62 ± 0.15	2.13 ± 0.1	104 ± 1	0.08 ± 0.01	211 ± 22	1.05 ± 0.05

ening was followed by a strain hardening region until the test samples broke. The values for the compressive modulus, E_c, compressive yield stress, σ_{yc}, the true yield strain, ε_{yc}, fracture stress, σ_f, and true fracture strain, ε_f, are given in Table 7. The fracture stress increased with the silica nanoparticle content, whereas the true fracture strain remains relatively constant. A sample of the unmodified epoxy was unloaded during the strain softening part of the response. The sample was sectioned, polished, and cross-polarised optical microscopy images were then taken. In Fig. 12 (inset), shear band yielding can be clearly observed in the partially loaded and polished section of the compressed region, hence shear band yielding in the process zone of the crack tip would be expected, initiating at the particles in the case of the silica nanoparticle-modified epoxies.

Single-edge-notch bend tests were conducted to investigate the effect of the silica content on the fracture energy and fracture toughness. The results are summarised in Table 7, and show that a small difference was measured in the fracture energy (177–211 J m^{-2}) or the fracture toughness (0.85–1.05 MPa$\sqrt{m}$), with the addition of up to 20 wt% of silica nanoparticles. This indicates that this fast-curing epoxy polymer was not readily toughenable using the silica nanoparticles.

Discussion

The kinetics of the epoxy polymer were studied and modelled with and without the addition of silica nanoparticles. The combination of the kinetic and heat transfer

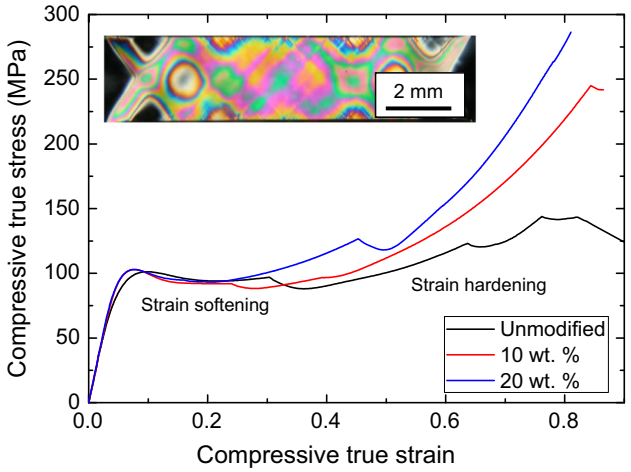


Fig. 12 Compressive true stress versus true strain of the unmodified and silica nanoparticle-modified epoxies, and (*inset*) a cross-polarised optical image of a section from the unmodified epoxy interrupted in the strain softening portion of the curve

models shows excellent agreement for the temperature progression and T_g measurements. The main challenge faced with such a fast-curing epoxy was to obtain proper isothermal measurements using DSC. Several possibilities were tried and a good set-up was achieved. As was observed from temperature measurement of the bulk epoxy plates, the temperature does not remain constant during isothermal curing. No influence of the silica nanoparticles was found on the kinetics itself, but the addition of the particles does reduce the total heat of the reaction (by a reduction in resin mass), which leads to a reduced exotherm during cure. This can prevent the material from damage or decomposition during the manufacturing of thick parts and/or the use of fast cure cycles, and hence leads to a more uniform T_g distribution over the thickness.

Rheological modelling was performed to predict the evolution of the viscosity during fibre impregnation. The influence of the silica nanoparticles on the initial viscosity was found to be small up to 20 wt% silica nanoparticles (a relatively high loading), making them very useful for heat reduction, without adversely affecting processing. A very high silica content (35.8 wt%) does lead, however, to a viscosity increase, which would cause difficulties during fabric impregnation in a composite material.

The lack of toughening was unexpected and inconsistent with published work for slow-curing epoxies [12, 14, 15]. Two major mechanisms have been widely recognised to provide toughening in particle-modified epoxies: namely (i) plastic shear bands and (ii) debonding of the matrix from the particles and subsequent plastic void growth of the epoxy. PSC tests show that the unmodified and silica-modified polymers do indeed strain soften and the polished sections provide evidence of shear bands. Likewise, observation of the plan view of fractured samples using cross-polarised light confirmed that shear bands were present in all samples. Scanning electron microscopy could not identify particle debonding and plastic void growth, hence the expected toughening would be modest due to energy absorption via shear band yielding alone, without particle debonding and void growth in the crack tip plastic zone. The level of interfacial adhesion can be quantified using the model of Vörös and Pukánszky [35, 36] to compute the proportionality constant, k, for interfacial stress transfer by assuming that the particles carry a load proportional to their volume fraction using stress averaging [12]. Interestingly, as the molecular weight between crosslinks was calculated to decrease with increasing silica nanoparticle content, the yield strength of the polymer network would be expected to decrease, with a superposition of stress increase interfacial stress transfer due to the silica nanoparticles in the measured compressive yield strength. Nevertheless, a value of $k = 1.05$ was calculated, which indicates that the silica nanoparticles are relatively well bonded to the epoxy and disregarding the effect of reduction in bulk polymer yield properties (where values of the range 0.46–1.88 were previously reported for k [12]).

The difference between the unmodified polymer and that with the addition of silica nanoparticles seems to be the degree to which the polymer exotherms (and its corresponding temperature overshoot, see Fig. 6). This may be demonstrated by observing the results shown in Table 3. The mould temperature, the corresponding measured T_g of the cured epoxy and the calculated T_g of the epoxy were recorded for different cure cycles from the centre and edge of the epoxy plates. Our findings indicate that (i) thinner epoxy plates have a lower exotherm and as expected T_g is consistently lower throughout the plate. It may be noted that the amine hardener starts to decompose at temperatures above 200 °C as would be the case for a 6-mm epoxy plate manufactured using a 100 °C mould temperature. (ii) The T_g at the edge of the plate is consistently lower than in the centre of the plate, as heat from the exothermic reaction is conducted away from the sample due to the thermal mass of the mould. (iii) The addition of silica particles results in a lower T_g (112 °C for the unmodified epoxy compared with 104 °C for 20 wt%. silica nanoparticles), which indicates that the epoxy network likely has a lower crosslink density.

Conclusions

The thermal, mechanical and fracture properties of a silica nanoparticle-modified fast-curing epoxy have been measured, and a kinetic and rheological model was successfully developed. There is a significant exotherm during curing

which causes a variation in properties across the thickness of cast plates. Hence the heat conduction equation was used to model the resin temperature during curing, enabling the degree of cure and the resultant T_g to be predicted. Comparison of the calculated T_g values with experimental data shows good agreement, and demonstrates the accuracy of the kinetic models. The addition of silica nanoparticles had no influence on the curing reaction itself, but it reduces the total heat of reaction, and hence reduces the exothermic reaction during cure. This makes the manufacturing of thick parts and the use of fast cure cycles more controllable.

The influence of the silica nanoparticles on the initial viscosity was found to be small with up to 20 wt% of silica. No additional toughening was obtained by the addition of silica nanoparticles. Shear band yielding was present in the samples, but there was no additional energy dissipation caused by the silica, and nanoparticle debonding and void growth were not observed.

Acknowledgements The authors would like to thank the EPSRC Centre for Innovative Manufacturing in Composites Grant Reference EP/1033513/1, Project Number RGS 109687, and the Commission for Technology and Innovation in Switzerland Grant 15828.1 PFEN-IW for funding this study. The authors would also like to thank Huntsman Advanced Materials, Switzerland, and Evonik Hanse, Germany, for supplying materials, plus Anton Paar Switzerland AG, Switzerland, for supporting the rheological measurements. The contributions of H.M. Chong, F. Leone, J. Studer, R. Strässle and P. Tsotra are gratefully acknowledged. Data supporting this publication can be obtained on request from adhesion.group@imperial.ac.uk.

Open Access This article is distributed under the terms of the Creative Commons Attribution 4.0 International License (http://creativecommons.org/licenses/by/4.0/), which permits unrestricted use, distribution, and reproduction in any medium, provided you give appropriate credit to the original author(s) and the source, provide a link to the Creative Commons license, and indicate if changes were made.

References

1. Bhat P, Merotte J, Simacek P, Advani SG (2009) Process analysis of compression resin transfer molding. Compos A 40(4):431–441
2. Karkanas PI, Partridge IK (2000) Cure modeling and monitoring of epoxy/amine resin systems. I. Cure kinetics modeling. J Appl Polym Sci 77(7):1419–1431
3. Yousefi A, Lafleur PG, Gauvin R (1997) Kinetic studies of thermoset cure reactions: a review. Polym Compos 18(2):157–168
4. Kiuna N, Lawrence CJ, Fontana QPV, Lee PD, Selerland T, Spelt PDM (2002) A model for resin viscosity during cure in the resin transfer moulding process. Compos A 33(11):1497–1503
5. Hardis R, Jessop JLP, Peters FE, Kessler MR (2013) Cure kinetics characterization and monitoring of an epoxy resin using DSC, Raman spectroscopy, and DEA. Compos A 49:100–108
6. Yang LF, Yao KD, Koh W (1999) Kinetics analysis of the curing reaction of fast cure epoxy prepregs. J Appl Polym Sci 73(8):1501–1508
7. Prime RB, Michalski C, Neag CM (2005) Kinetic analysis of a fast reacting thermoset system. Thermochim Acta 429(2): 213–217
8. Guo Z-S, Du S, Zhang B (2005) Temperature field of thick thermoset composite laminates during cure process. Compos Sci Technol 65(3):517–523
9. Zhang J, Xu Y, Huang P (2009) Effect of cure cycle on curing process and hardness for epoxy resin. Express Polym Lett 3(9): 534–541
10. Nelson J, Hine AM, Goetz DP, Sedgwick P, Lowe RH, Rexeisen E, King RE, Aitken C, Pham Q (2013) Properties and applications of nanosilica-modified tooling prepregs. SAMPE Journal 49:7–17
11. Sprenger S, Kothmann MH, Altstaedt V (2014) Carbon fiber-reinforced composites using an epoxy resin matrix modified with reactive liquid rubber and silica nanoparticles. Compos Sci Technol 105:86–95. doi:10.1016/j.compscitech.2014.10.003
12. Hsieh TH, Kinloch AJ, Masania K, Taylor AC, Sprenger S (2010) The mechanisms and mechanics of the toughening of epoxy polymers modified with silica nanoparticles. Polymer 51(26): 6284–6294. doi:10.1016/j.polymer.2010.10.048
13. Giannakopoulos I, Masania K, Taylor AC (2011) Toughening of epoxy using core-shell particles. J Mater Sci 46(2):327–338. doi:10.1007/s10853-010-4816-6
14. Hsieh TH, Kinloch AJ, Masania K, Sohn Lee J, Taylor AC, Sprenger S (2010) The toughness of epoxy polymers and fibre composites modified with rubber microparticles and silica nanoparticles. J Mater Sci 45(5):1193–1210. doi:10.1007/s10853-009-4064-9
15. Bray DJ, Dittanet P, Guild FJ, Kinloch AJ, Masania K, Pearson RA, Taylor AC (2013) The modelling of the toughening of epoxy polymers via silica nanoparticles: the effects of volume fraction and particle size. Polymer 54(26):7022–7032. doi:10.1016/j.polymer.2013.10.034
16. Blackman BRK, Kinloch AJ, Sohn Lee J, Taylor AC, Agarwal R, Schueneman G, Sprenger S (2007) The fracture and fatigue behaviour of nano-modified epoxy polymers. J Mater Sci 42(16):7049–7051. doi:10.1007/s10853-007-1768-6
17. Kinloch AJ, Masania K, Taylor AC, Sprenger S, Egan D (2008) The fracture of glass-fibre reinforced epoxy composites using nanoparticle-modified matrices. J Mater Sci 43(3):1151–1154. doi:10.1007/s10853-007-2390-3
18. Kinloch AJ, Mohammed RD, Taylor AC, Sprenger S, Egan D (2006) The interlaminar toughness of carbon-fibre reinforced plastic composites using 'hybrid-toughened' matrices. J Mater Sci 41(15):5043–5046. doi:10.1007/s10853-006-0130-8
19. Nielsen LE (1969) Cross-linking effect on physical properties of polymers. J Macromol Sci 3:69–103. doi:10.1080/15583726908545897
20. Bellenger V, Verdu J, Morel E (1987) Effect of structure on glass transition temperature of amine crosslinked epoxies. J Polym Sci 25(6):1219–1234
21. Pearson RA, Yee AF (1989) Toughening mechanisms in elastomer-modified epoxies. 3. The effect of cross-link density. J Mater Sci 24(7):2571–2580. doi:10.1007/BF01174528
22. BS-EN-ISO-527-2, Plastics: determination of tensile properties. Part 2: test conditions for moulding and extrusion plastics, 2012, BSI, London
23. Williams J, Ford H (1964) Stress-strain relationships for some unreinforced plastics. J Mech Eng Sci 6(4):405–417. doi:10.1243/JMES_JOUR_1964_006_055_02
24. ASTM-D5045-99, Standard test methods for plane-strain fracture toughness and strain energy release rate of plastic materials, 2007, American Society for Testing and Materials, West Conshohocken

25. Vyazovkin S, Wight CA (1999) Model-free and model-fitting approaches to kinetic analysis of isothermal and nonisothermal data. Thermochim Acta 340:53–68
26. Vyazovkin S (2006) Model-free kinetics. J Therm Anal Calorim 83(1):45–51
27. Kandelbauer A (2009) Wuzella, G, Mahendran, A, Taudes, I, Widsten, P, Model-free kinetic analysis of melamine–formaldehyde resin cure. Chem Eng J 152(2):556–565
28. Rivero G, Pettarin V, Vázquez A, Manfredi LB (2011) Curing kinetics of a furan resin and its nanocomposites. Thermochim Acta 516(1):79–87
29. Bailleul J-L, Delaunay D, Jarny Y (1996) Determination of temperature variable properties of composite materials: methodology and experimental results. J Reinf Plast Compos 15(5):479–496
30. Ruiz E, Trochu F (2005) Thermomechanical properties during cure of glass-polyester RTM composites: elastic and viscoelastic modeling. J Compos Mater 39(10):881–916
31. DiBenedetto AT (1987) Prediction of the glass transition temperature of polymers: a model based on the principle of corresponding states. J Polym Sci 25(9):1949–1969
32. Lewis RW, Nithiarasu P, Seetharamu K (2004) Fundamentals of finite element method for heat and fluid flow. Wiley, Chichester
33. Wong CP, Bollampally RS (1999) Thermal conductivity, elastic modulus, and coefficient of thermal expansion of polymer composites filled with ceramic particles for electronic packaging. J Appl Polym Sci 74(14):3396–3403
34. Bray DJ, Gilmour SG, Guild FJ, Hsieh TH, Masania K, Taylor AC (2011) Quantifying nanoparticle dispersion: application of the Delaunay network for objective analysis of sample micrographs. J Mater Sci 46(19):6437–6452. doi:10.1007/s10853-011-5615-4
35. Vörös G, Pukánszky B (1995) Stress distribution in particulate filled composites and its effect on micromechanical deformation. J Mater Sci 30(16):4171–4178. doi:10.1007/BF00360726
36. Pukánszky B, Vörös G (1996) Stress distribution around inclusions, interaction, and mechanical properties of particulate-filled composites. Polym Compos 17(3):384–392. doi:10.1002/pc.10625
37. Ashby MF, Jones DR, Heinzelmann M (2006) Werkstoffe: Eigenschaften, Mechanismen und Anwendungen. Elsevier, Spektrum Akad, Verlag